Journal of Renewable and Sustainable Energy

RESEARCH ARTICLE | JULY 24 2024

Wind plant wake losses: Disconnect between turbine actuation and control of plant wakes with engineering wake models

Special Collection: Preparatory work for the American Wake Experiment (AWAKEN)

Ryan Scott ; Nicholas Hamilton ; Raúl Bayoán Cal ; Patrick Moriarty

J. Renewable Sustainable Energy 16, 043303 (2024)
https://doi.org/10.1063/5.0207013

Journal of Renewable and Sustainable Energy ARTICLE pubs.aip.org/aip/rse

Wind plant wake losses: Disconnect between turbine actuation and control of plant wakes with engineering wake models

Cite as: J. Renewable Sustainable Energy **16**, 043303 (2024); doi: 10.1063/5.0207013
Submitted: 5 March 2024 · Accepted: 1 July 2024 ·
Published Online: 24 July 2024

View Online Export Citation CrossMark

Ryan Scott,[1,2,a)] Nicholas Hamilton,[2] Raúl Bayoán Cal,[1] and Patrick Moriarty[2]

AFFILIATIONS

[1]Department of Mechanical Engineering, Portland State University, Portland, Oregon 97201, USA
[2]National Renewable Energy Laboratory, Golden, Colorado 80401, USA

Note: This article is part of the special issue Preparatory Work for the American Wake Experiment (AWAKEN)
[a)]**Author to whom correspondence should be addressed:** ryan.scott@nrel.gov and rhs2@pdx.edu

ABSTRACT

Wake losses from neighboring plants may become a major factor in wind plant design and control as additional plants are constructed in areas with high wind resource availability. Because plant wakes span a large range of physical scales, from turbine rotor diameter to tens of kilometers, it is unclear whether conventional wake models or turbine control strategies are effective at the plant scale. Wake steering and axial induction control are evaluated in the current work as means of reducing the impact of neighboring wind plants on power and levelized cost of electricity. FLOw Redirection and Induction in Steady State (FLORIS) simulations were performed with the Gauss–Curl Hybrid and TurbOPark wake models as well as two operation and maintenance models to investigate control setpoint sensitivity to wake representation and economic factors. Both wake models estimate losses across a range of atmospheric conditions, although the wake loss magnitude is dependent on the wake model. Annual energy production and levelized cost of electricity are driven by wind direction frequency, with frequently aligned plants experiencing the greatest losses. However, both wake steering and axial induction are unable to mitigate the impact of upstream plants. Wake steering is constrained by plant geometry, since wake displacement is much less than the plant wake width, while axial induction requires curtailing the majority of turbines in upstream plants. Individual turbine strategies are limited by their effective scale and model representation. New wake models that include plant-scale physics are needed to facilitate the design of effective plant wake control strategies.

I. INTRODUCTION

Installed wind energy capacity continues to expand with the global demand for renewable energy.[1,2] However, regional wind plant development is a decentralized process involving multiple stakeholders with independent interest and timelines.[3] As new plants are constructed in areas with high wind resource availability, additional growth decreases the distance between neighboring plants. Plant wakes can extend 50 km downstream,[3–5] yet 90% of wind plants in the United States are located within 40 km of a neighboring plant.[3] Consequently, wind plants often operate in a wake region imposed by one or more neighboring wind plants.

Plant wakes reduce the energy available to neighboring plants, resulting in lower annual energy production (AEP).[3–11] Although exact operating costs are site-specific and proprietary, the combined costs of neighbor-induced wake losses averaged to an annual loss of $2.0 ± 1.29 million for the Roscoe Wind Farm Project in Texas.[3] In addition, wakes introduce turbulence into the downstream flow, which increases fatigue damage.[12–17] The extent of a plant wake varies with atmospheric conditions, turbine arrangement within the plant, and spacing between plants.[4,5,8–11] At the same time, wind turbines are most sensitive to wake losses when operating below their rated wind speed.[6] Stable conditions with low ambient turbulence intensity allow wakes to propagate far downstream compared to unstable conditions.[4,5,11]

Wind plant wakes are governed by a combination of layout-specific interactions between turbine clusters and atmospheric conditions.[5,7,11,18] While control strategies such as yaw-based wake steering[8,10,19–25] and induction control[26–29] allow plant operators to improve

net efficiency while utilizing the existing infrastructure, the majority of work on mitigating wake losses has focused on characterizing the fundamental dynamics of the wake from a single turbine or optimizing the performance of a single plant.[8] As such, it is unclear how well single-wake models and contemporary control strategies extend to multiplant systems. Foloppe *et al.*[10] found yaw-based wake steering improved the regional power output for the Belgian offshore wind farm zone. Stieren and Stevens[9] showed optimizing an upstream farm layout leads to a strong aggregate plant wake, which reduces the energy available to its downstream neighbor. Because conventional control strategies rely on modifying individual turbines, these strategies may be constrained to the subset of conditions where single wakes have an outsized impact on neighboring turbines. Differences in operating costs between neighboring wind plants add an additional layer of uncertainty to estimating the impact of plant wakes. Capital expenses depend on the turbine model, installation date, and financing at the time of installation. Operating costs are subject to numerous external factors and can vary as the turbine ages. Power purchase agreements (PPAs) are operator-specific and subject to negotiations as well as prevailing market rates. Yet economic values are often presented as national or regional averages.[2,30] These complications are compounded by the limitations of current modeling tools. Large eddy simulations are too computationally expensive to optimize control strategies over a large number of turbines or wide range of atmospheric conditions. Engineering wake models are less expensive than high-fidelity simulations and capable of designing effective control strategies.[22,25] However, these tools are designed to capture individual wake dynamics and omit relevant physics at the regional scale, such as gravitational waves, plant blockage, internal boundary layer formation, and atmospheric stability.[31,32]

The current work considers contemporary control strategies as means of reducing neighbor-induced wake losses through a series of turbine setpoint optimizations. Wake loss estimates are obtained from FLOw Redirection and Induction in Steady State (FLORIS)[33] simulations with two wake models across a range of measured atmospheric conditions to highlight the impacts of inflow conditions and wake model selection. Wake steering and axial induction control are compared to baseline operation to assess their potential for mitigating wake losses from neighboring plants. Specifics on modeling approach, simulation setup, and the optimization functions are detailed in Sec. II. Results are presented and discussed in Sec. III. Concluding remarks and suggestions for future studies follow in Sec. IV.

II. METHODS

A. AWAKEN site

The five plants under observation in the American WAKE experimeNt (AWAKEN) field campaign are a suitable test system, as these plants operate in close proximity and contain multiple turbine types with different layout strategies.[34] In addition, two main scientific objectives of the AWAKEN project are characterizing wind plant wake development and assessing the effectiveness of turbine controls on mitigating wake interactions within turbine clusters. AWAKEN plant specifications (Table I) including turbine model and location were obtained from the United States Geological Survey Wind Turbine Database.[35] Turbine models were created from an open-source 2.8 MW reference turbine[36] with the WISDEM/WEIS toolkit.[37]

B. Atmospheric conditions

Atmospheric conditions spanning 2021 were obtained from atmospheric radiation measurement (ARM) instruments located at the Southern Great Plains Central Facility[38–44] (Fig. 1). Atmospheric quantities, including wind speed, wind direction, turbulence intensity, shear exponent, and Monin–Obukhov stability parameters, were reported as

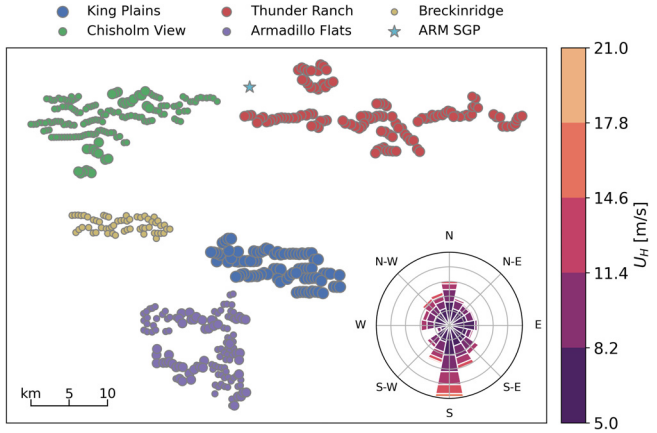

FIG. 1. AWAKEN plants with Atmospheric Radiation Measurement Southern Great Plains Central Facility location (star) and wind rose of atmospheric conditions. Marker size is relative to turbine nameplate capacity.

TABLE I. AWAKEN wind plant specifications from the United States Geological Survey Wind Turbine Database.[35] The study site is composed of 558 General Electric (GE) turbines with six unique turbine models.

Plant name	Operation year	Rated power (MW)	Total turbines	Turbine model	Rotor diameter (m)	Hub height (m)
Chisholm View	2012	300	167	140 × GE 1.68 MW	82.5	80
				27 × GE 2.4 MW	107	80
Breckinridge	2015	96.9	57	57 × GE 1.7 MW	103	80
Thunder Ranch	2017	297.8	120	109 × GE 2.5 MW	116	90
				11 × GE 2.3 MW	116	80
Armadillo Flats	2018	241.8	126	80 × GE 1.7 MW	103	80
				46 × GE 2.3 MW	116	90
King Plains	2020	248.2	88	88 × GE 2.82 MW	127	89

30-min averages at 25 and 60 m elevations. ARM data were compared to instrumentation throughout the AWAKEN site to check for variations at hub-height. Wind direction and turbulence intensity were in agreement although wind speed differed and was extrapolated from 60 m up to 90 m with a power law. Overall, the 2021 data compare well with the 2010–2020 averages.[45] The annual mean wind speed is 8.8 m/s with a corresponding mean inflow wind direction of 177.8°, turbulence intensity of 11.2%, and shear exponent of 0.19. The majority of wind to the AWAKEN site arrives from the south (59.7%) while winds from the East of West are relatively uncommon. For FLORIS simulations, wind speed was discretized into 1 m/s intervals from 5 to 21 m/s, wind direction into 10° intervals from 0° to 350°, and turbulence intensity into 2.5% intervals from 5% to 25%. Wind speed, direction, and turbulence intensity frequencies were computed from the number of occurrences relative to the total number of observations. Shear exponent did not vary with the other atmospheric variables and was set to a canonical value of 0.2 rather than included as an additional input parameter. In addition, wind speeds and turbulence intensities with inflow wind directions between $100\pm10°$ and $270\pm20°$ were removed since ARM facilities are impacted by Chisholm View and Thunder Ranch wind plants.[45]

C. Economic data

Financial data for the Southern Great Plains region[30] were used to inform the optimization efforts (Table II). Capital expenses (CapEx), operating expenses (OpEx), and fixed charge rate (FCR) represent the most recent estimate (2022) of national averages for land-based turbines in the United States.[30] Power purchase agreement (PPA) data are the most recent (2022) estimates for wind plants in the U.S. Southwest Power Pool region.[2] Because economic data are confidential, costs were computed for each plant on a per-turbine basis using the best estimate for a typical land-based turbine.[30]

D. Turbine O&M models

Heightened wind speeds and turbulence intensities lead to large loads and reduce turbine fatigue lifetimes, which increases turbine operation and maintenance (O&M) costs.[12–17] Recent efforts have produced a variety of models for estimating fatigue damage.[12,15–17] However, the relationship between fatigue loads and atmospheric trends is dependent on individual turbine characteristics and the time history of flow conditions at each turbine. While the models developed by Stanley *et al.*[17] and Natarajan[16] provide means for estimating time histories for specific conditions, implementing this functionality in FLORIS is beyond the scope of the current study. Furthermore, the relationship between fatigue damage and turbine operating costs is poorly defined, as much of this information is proprietary. In light of these limitations, two methods are employed for representing the effects of turbine wear on O&M expenses. Because FLORIS simulations are steady state, both methods are designed to approximate turbine wear at a specific operating condition. Annual wear is approximated by weighting the output of each model by the frequency of the corresponding atmospheric condition in a similar manner to AEP calculations.

The first model is designed to capture the effects of wind speed and turbulence intensity on turbine fatigue life through the L_{10} metric, where L_{10} represents the estimated time or number of rotations until a drivetrain bearing reaches 10% probability of failure.[46–48] A two-step fit is performed to map a family of logistic curves to the unwaked L_{10} data from Clark *et al.*[15] First, the minimum turbine lifetime is estimated from a linear fit of turbulence intensity and L_{10} yielding $L_{10\text{min}} = -4.9TI + 2.95$, where TI is the hub-height turbulence intensity. Next, $L_{10\text{min}}$ is substituted into a logistic function to find L_{10},

$$L_{10} = L_{10\text{min}} + \frac{L_{10\text{max}} - L_{10\text{min}}}{1 + e^{a(U_H - b)}}, \tag{1}$$

where U_H is the hub-height velocity, $a = 0.85$ and $b = 7.75$ are fit coefficients, and $L_{10\text{max}} = 25$ is the design lifetime in years following Clark *et al.*[15] The logistic function agrees well with the published data and provides a smooth mapping from turbine operating conditions to bearing life expectancy (Fig. 2).

The second model considers turbine loading rather than bearing wear and is derived from the definition of thrust coefficient,

$$F_T = \frac{1}{2} C_T \rho A U_A^2, \tag{2}$$

where C_T is the turbine thrust coefficient, ρ is the air density, A the rotor area, and U_A the rotor-averaged velocity. Although rotor loads are an instantaneous structural response to fluid–blade interactions, this representation abstracts individual component lifetimes by assuming turbine O&M costs scale with wind speed across the rotor and turbine operation.

E. Optimization functions

External wake losses (EWLs) from neighboring plants are quantified through the ratio of turbine performance with and without neighboring plants. This ratio isolates the impact of external plant wakes on turbine operation by canceling internal wake losses between turbines within a plant. Two cost functions are considered for mitigating EWL by either improving plant power output or reducing levelized cost of electricity (LCOE). In addition, two subfunctions were implemented within each cost function to test optimizer sensitivity to turbine selection. In the first subfunction, the optimizer was allowed to control any turbine individually, and the cost function was evaluated across all turbines in the domain. In the second, the optimizer was again allowed to control any turbine, but the cost function was only computed for turbines with known EWL. A turbine was designated as having EWL if the power output was reduced by at least 0.5% from the presence of an upstream plant.

The power cost function seeks to reduce EWL by minimizing the difference in power between plant operation with and without upstream neighbors,

$$\min_x : 1 - \sum_{i=1}^{n} \frac{P_{i,x}}{P_{i,0}}, \tag{3}$$

where n is the total number of turbines, $P_{i,x}$ is the power of turbine i at control setting x, and 0 denotes the reference power of the turbine

TABLE II. Economic data for (1) US national average land-based turbine costs[30] and (2) regional average purchase agreement price.[2]

CapEx[1] (US$/kW h)	OpEx[1] (US$/kW h)	FCR[1] (%)	PPA[2] (US$/MW h)
1462	43	5.78	20

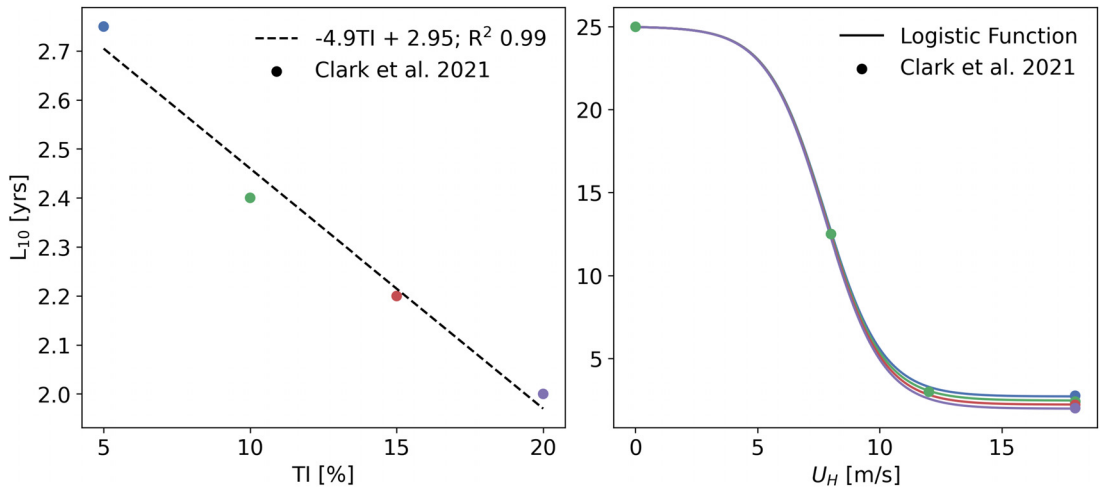

FIG. 2. Linear fit of turbulence intensity (left) and corresponding family of logistic curves (right) for bearing L_{10} lifetime in years with reference data from Clark *et al.*[15]

under typical operation in the absence of neighboring plants. This cost function returns the optimal per-turbine yaw or axial induction setting for each atmospheric condition.

Optimizing power output alone neglects changes in turbine O&M costs from implementing control strategies as well as differences in installed capacity and operating costs between plants. LCOE includes this information and is defined here as

$$\text{LCOE} = \sum_{i=1} \mathcal{F}_i \sum_{j=1}^{n} \frac{\text{FCR} \cdot \text{CapEx}_j + \text{OpEx}_j}{\text{CF}_{j,x} \cdot 8,760}, \tag{4}$$

where $\mathcal{F}_i$ is the frequency of atmospheric condition i, FCR is the fixed charged rate, CapEx_j is the capital cost of turbine j in \$/kW, OpEx_j is the O&M cost for turbine j in \$/kW, $\text{CF}_{j,x}$ is the capacity factor of turbine j operating at control setting x, and 8760 scales steady-state power estimates to the annual capacity factor for the current atmospheric condition. Because the precise O&M costs under different operating strategies are not available for the turbines at the AWAKEN site, these effects are represented through the ratio of L_{10} or F_T under active control to typical operation given by

$$R_j = \frac{L_{10,0}}{L_{10,x}} \quad \text{or} \quad R_j = \frac{F_{T,x}}{F_{T,0}}, \tag{5}$$

where $L_{10,0}$ is the L_{10} bearing lifetime under typical operation, $L_{10,x}$ is bearing lifetime at control setting x, $F_{T,0}$ is the rotor-averaged load force under typical operation, and $F_{T,x}$ is the rotor-averaged load force at control setting x. For a turbine j at control setting x, OpEx_j becomes $\text{OpEx}(x)_j = R_j \cdot \text{OpEx}_j$. With this formulation, any reduction in bearing lifetime or increased force on the turbine will raise O&M costs, while improved bearing wear or reduced loads lower O&M costs. The LCOE cost function for a specific atmospheric condition i is then

$$\min_x : \sum_{j=1}^{n} \frac{\text{LCOE}_{j,x}}{\text{LCOE}_{j,0}} - 1, \tag{6}$$

where, as before, j denotes the turbine in question, 0 indicates typical operation in the absence of neighboring plants, x is the active control setting, and the cost function returns x as the optimal per-turbine yaw or axial induction setting for each atmospheric condition.

F. Modeling approach

Wind plant simulations were performed with FLORIS version 3.1.[33] Although engineering wake models can underestimate the plant wake velocity deficit far downstream,[6,7,49] the large number of iterations needed to evaluate control strategies necessitates a computationally efficient approach. Two wake models were used in the study to perform a direct comparison between models and facilitate both yaw and axial induction control. The Gauss–Curl Hybrid (GCH) was selected for its physical fidelity representing yawed wakes[50] and the TurbOPark model was selected as it has demonstrated good agreement with measured plant performance in offshore settings.[7,49] The GCH model is based on a Gaussian wake profile[51,52] and includes the effect of the counter-rotating vortex from yaw misalignment on wake deflection and recovery.[50,53,54] Wakes in the GCH model are represented on a grid and wake merging is computed via sum of squares to avoid negative velocity deficits. The TurbOPark model was designed to capture far wake development and employs a top hat velocity deficit,[55] which includes the effects of local turbulence intensity on wake expansion.[7] Velocity deficits in the TurbOPark model are treated as points that are linearly superimposed on downstream turbines. Optimal agreement using the TurbOPark model was realized by increasing FLORIS turbulence intensity by a constant 2.5% and setting the wake expansion parameter, A, to 0.2.

Optimizations were performed for each atmospheric condition using the L-BFGS-B method,[56,57] as implemented in SciPy version 1.10.1.[58] Yaw angles were optimized between 0° and 25° at an inflow velocity of 8 m/s. Optimal yaw angles were linearly interpolated toward 0 at 5 and 11 m/s to mimic a utility-scale yaw steering controller.[22] Axial induction was modeled by weighting each turbine's thrust coefficient for a given wind speed by a scalar parameter $0 \leq x \leq 1$, where 0 is shut down and 1 is normal operation. This approach allows tuning individual thrust coefficients and is implemented in a development version of FLORIS 3.1.[59] At the time of writing, yaw control is not

TABLE III. Suite of FLORIS cases as determined by simulation objective (A), wake model (B), turbine selection (C), controls strategy (D), and turbine O&M model (E).

A	Wake losses				Power optimization								LCOE optimization											
B	GCH		TurbOPark		GCH				TurbOPark				GCH								TurbOPark			
C					All		EWL		All		EWL		All				EWL				All		EWL	
D					Yaw		C_T		Yaw		C_T		C_T		C_T		Yaw		C_T		Yaw		C_T	
E													F_T	L_{10}	F_T	L_{10}	F_T	L_{10}	F_T	L_{10}	F_T	L_{10}	F_T	L_{10}

implemented for the TurbOPark wake model, so direct comparisons between wake models are limited to losses among plants and axial induction control. In total, 20 cases with 558 turbines and 1554 atmospheric conditions each were evaluated in FLORIS (Table III).

III. RESULTS AND DISCUSSION

A. External wake losses at the AWAKEN site

Wind plants at the AWAKEN site interact with their neighbors across a range of atmospheric conditions. EWLs occur for 48% of possible inflow conditions with both wake models. Losses are most pronounced at moderate wind speeds between 5 and 9 m/s when turbines are below rated power and when wake recovery is limited by low ambient turbulence intensity below 7.5% (Fig. 3, top). Both wake models predict similar EWL trends in response to atmospheric conditions. However, EWL estimates using the TurbOPark model are approximately twice the magnitude of those from GCH under the same conditions. This discrepancy is expected as the TurbOPark model was designed to capture far wake evolution over several kilometers,[7,49] while the GCH model was developed to capture dominant physics including the counter-rotating vortex pair from misalignment within typical plant spacings.[50]

Turbines in close proximity to neighboring plants experience high EWL regardless of atmospheric conditions since wake recovery is primarily dependent on separation distance. EWLs are concentrated in the outer edges of each wind plant (Fig. 4). This indicates internal wake losses dominate for the remaining turbines over the momentum deficit created by an upstream plant. In addition, plants with many neighbors, such as Breckinridge and King Plains, are more likely to be in a wake for a given wind direction, resulting in EWL across a greater range of wind directions. The arrangement of plants at the AWAKEN site leads to EWL across 75% of inflow wind directions at Breckinridge and King Plains, while Armadillo Flats, Chisholm View, and Thunder Ranch experience EWL under 40% of inflow directions (Fig. 3, bottom).

Changes in AEP and LCOE from the presence of a neighboring plant are driven by how often high-loss conditions occur. Although

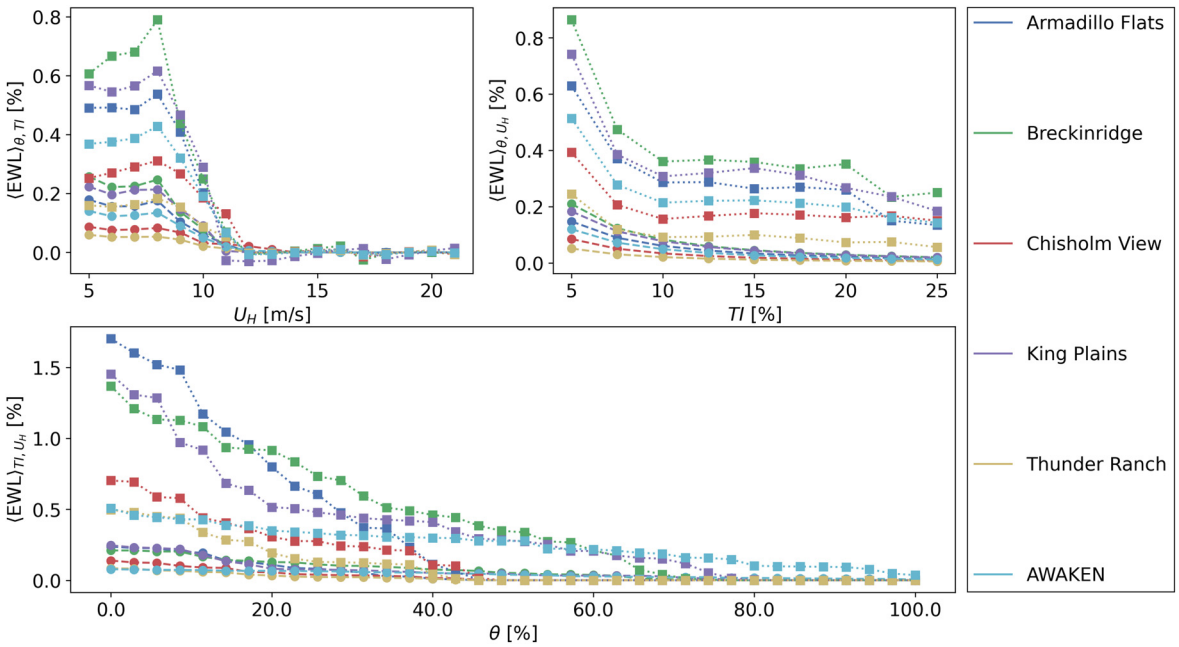

FIG. 3. Mean plant external wake losses in response to wind speed (top left), turbulence intensity (top right), and percentage of wind directions under which external wake losses occur (bottom) for the GCH (dashed circles) and TurbOPark (dotted squares) wake models. Here, AWAKEN denotes the average EWL across the five wind plants in the study site.

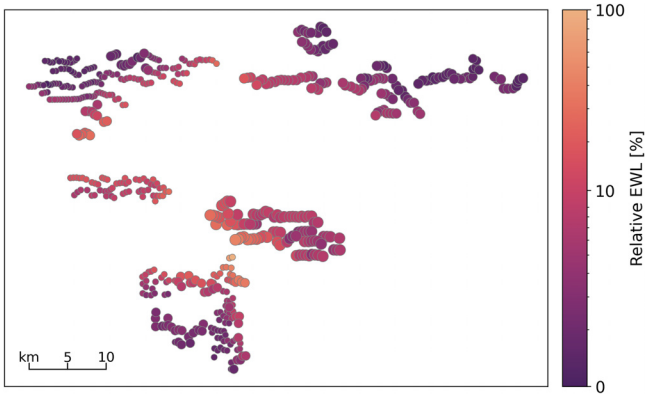

FIG. 4. Relative EWL across all atmospheric conditions. Color denotes wake loss magnitude as a percentage relative to other turbines with EWL. Size is relative to turbine nameplate capacity.

low wind speeds and turbulence intensity exacerbate EWL, wind direction frequency is the primary driver, as plants aligned with common wind directions incur the greatest losses (Fig. 5, top). Because the majority of wind to the AWAKEN site arrives from the south, King Plains, Chisholm View, and Breckinridge experience the bulk of AEP losses. Although Armadillo Flats can experience high EWL from its proximity to neighboring plants, those wind directions are infrequent, leading to a lower AEP loss compared to its neighbors. Thunder Ranch is distant from neighboring plants and has the lowest AEP increase. This trend is reflected in plant LCOE, where frequently aligned plants experience the greatest cost increase (Fig. 5, bottom). Turbine quantity, size, and nameplate capacity also influence LCOE through plant capacity factor. The increase in LCOE for Armadillo Flats is twice its average EWL, while the changes in LCOE for Breckinridge, Chisholm View, and King Plains are all comparable to their average EWL. Thunder Ranch has a negligible increase in LCOE relative to its average EWL due to a combination of its location relative to the other plants during the most frequent wind directions, large number of turbines, and high per-turbine capacity factor.

B. Power optimization

Power optimizations were performed for each cost function, wake model, and turbine selection function by finding for the optimal per-turbine yaw angle or induction setting, assuming steady atmospheric conditions. It is important to note the power objective function seeks to minimize the disruption caused by upstream plants rather than maximize total power output across all plants at the AWAKEN site. While wake steering has been shown to improve performance in dense plant arrangements,[10] the current study focuses on external rather than internal wake losses, as the distance between plants at the AWAKEN site allows individual wakes to merge into an aggregate plant wake. This distinction has immediate ramifications: Both yaw-based wake steering and axial induction are unable to reduce EWL from neighboring plants.

Including upstream plants in the cost function leads to no change in yaw or thrust setting, regardless of the atmospheric condition or wake model as the losses experienced by upstream plants surpass the reduction in EWL of their downstream neighbors. At the plant scale, key problems arise at the plant scale that limit the effectiveness of turbine controls as a means to reduce EWL. First, wake displacement from yaw is on the order of rotor diameter, while an aggregate plant wake can be measured in kilometers, depending on the turbine layout.

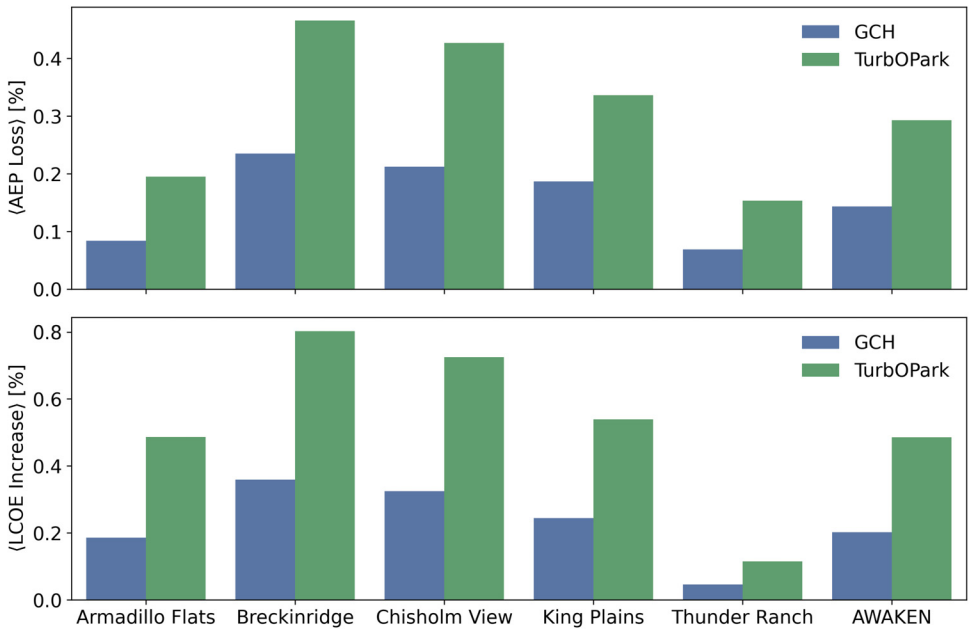

FIG. 5. Baseline AEP losses per plant (top) and increase to LCOE (bottom) due to EWL for both wake models. Here, AWAKEN shows the average AEP loss and LCOE increase across the five wind plants in the study site.

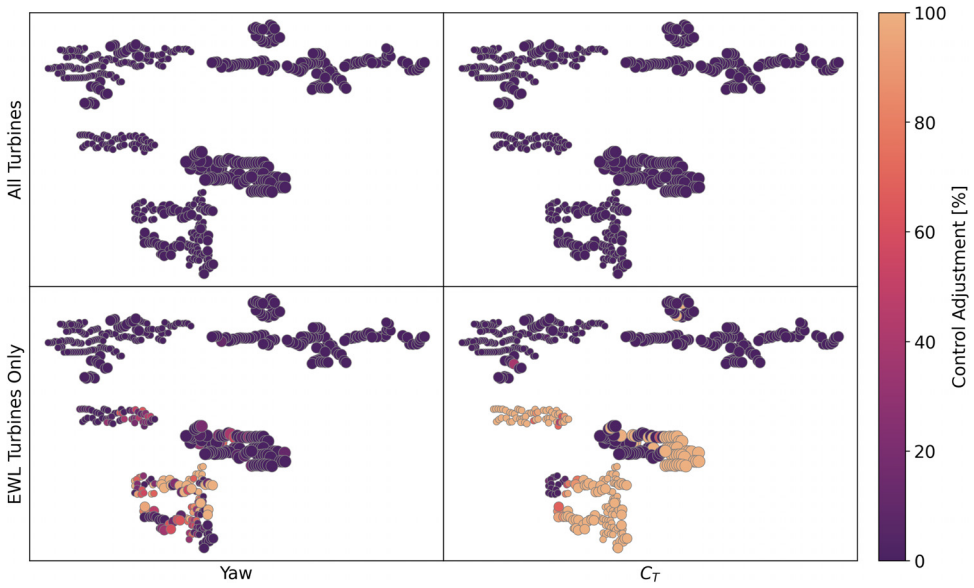

FIG. 6. Optimal turbine yaw (left column) and thrust coefficient weight (right column) for an inflow of 7 m/s from 200° at 5% ambient turbulence intensity. Control adjustment denotes the degree of yaw between 0° and 25° or thrust coefficient reduction from 0% to 100%. For induction control, 0% is typical operation and 100% is complete shutdown.

When the distance between plants exceeds typical row spacing, or when the upstream plant is large, individual turbine wakes merge into a bulk momentum deficit. As a consequence, wake steering is limited to the subset of atmospheric conditions and plant layouts where individual turbine wakes have an outsized influence on EWL. Furthermore, the version of FLORIS used in this study generates steady-state snapshots of turbine operation and the resulting wake field, assuming homogeneous inflow conditions. Including heterogeneous wind speeds and wind directions, as well as mesoscale coupling for plant blockage and boundary layer feedback, would greatly improve plant wake representation.

Neglecting losses in upstream turbines and only considering the change in performance for the subset of turbines with EWL under typical conditions allows the optimizer to identify beneficial yaw and thrust settings for downstream plants. However, these settings are detrimental to regional power output, as they explicitly ignore power losses in upstream plants. For the majority of inflow wind directions, the number of turbines required to reduce EWL at a downstream plant disproportionately impacts any upstream neighbors. When optimizing axial induction for the subset of turbines with EWL, the optimal result was to deactivate any upstream turbines by setting their thrust coefficient to 0 (Fig. 6). This outcome suggests axial induction control is ill-suited to addressing power losses between neighboring plants.

C. LCOE optimization

LCOE optimizations were performed in the same manner as power optimizations, with the addition of two models for turbine O&M costs based on L_{10} bearing lifetime and rotor-averaged thrust force F_T. As before, it is important to note the goal of these optimizations is to mitigate the additional costs incurred from EWL, as opposed to minimizing LCOE within plants. Despite including turbine O&M costs in the optimizations, neither strategy lowers EWL-driven LCOE.

Including upstream plants in the cost function leads to no change in turbine operation as power losses from implementing yaw or induction control in the upstream plants outweigh the benefits to their downstream neighbors. Omitting the LCOE of upstream turbines allows the optimizer to yaw or shut down turbines as needed to mitigate EWL-based LCOE. Again, these solutions are detrimental to regional performance, as the increased LCOE due to power losses in upstream plants exceeds the cost savings of their downstream neighbors. Although the turbine O&M models provide the optimizer with an additional degree of freedom, LCOE is more sensitive to changes in capacity factor than operating costs.

The cost function ratio is introduced to quantify the impact of controls strategy and O&M model on the proportion of turbines selected for control. This ratio is defined as the number of turbines selected for control by a given function relative to the total number of turbines selected for control at the AWAKEN site. Of the two control strategies, wake steering affects fewer turbines and is selected less often than axial induction (Fig. 7). With wake steering, a similar number of turbines are yawed across cost functions and turbine O&M models. In comparison, large portions of the AWAKEN site are selected for induction control, as this strategy allows the optimizer to disable any upstream turbines to reduce EWL, as discussed previously (Fig. 6). In particular, the L_{10} bearing lifetime O&M model leads to unrealistic behavior where all of the turbines are selected for induction control. For example, when 5% of the turbines are controlled, 15% of the time it is to improve power with yaw, 35% to improve LCOE with yaw using the F_T model, 15% to improve LCOE with yaw using the L_{10} model, 25% to improve power with induction control, and the remaining 10% to improve LCOE with induction control using the F_T model. When the optimizer chooses to control 95% of the turbines, none are

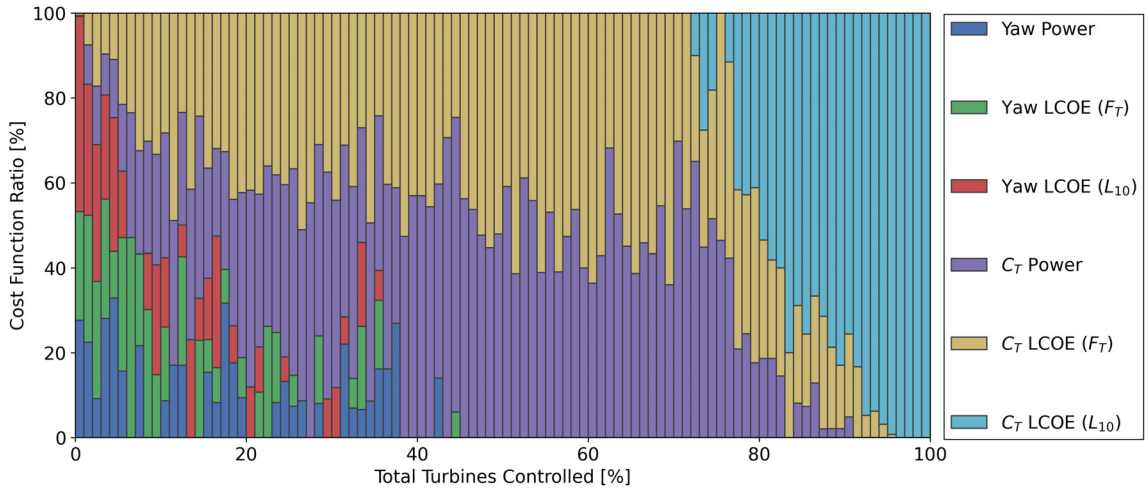

FIG. 7. Percentage of turbines in the AWAKEN site selected for either wake steering or axial induction control by cost function and turbine O&M model. Cost function ratio is computed for each bin as the proportion of turbines chosen for control by a given function.

yawed, approximately 5% of the time turbines are induction controlled to improve LCOE with the F_T model, and 95% are to improve LCOE with induction control using the L_{10} model. Because operating costs due to bearing wear increase with velocity in the L_{10} model, this formulation has the unintended consequence of incentivizing thrust control regardless of EWL.

Optimization surfaces show how LCOE varies relative to rated operation across O&M costs and capacity factor combinations (Fig. 8). LCOE optimizations are driven by turbine power output, with O&M models providing an incentive to lower operating costs above rated power. Optimizations are constrained by capacity factor, since LCOE behaves like $1/x$ below rated power (Fig. 8, bottom). Above rated power, the O&M models are limited by only representing a single component of turbine wear. Because both models are primarily functions of hub-height velocity, they are in competition with power output during the optimization process. Under the L_{10} function, optimal LCOE is found by improving bearing lifetime at or above rated power (Fig. 8, left column). Since bearing wear increases with velocity, this model disincentivizes yawing upstream turbines or reducing their thrust to mitigate wake losses. Paradoxically, operating in the wake of an upstream plant is the optimal strategy when only considering bearing wear. Under the F_T function, optimal LCOE is achieved by reducing thrust force on the rotor while preserving power output (Fig. 8, right column). Because peak thrust occurs near rated wind speed, increasing velocity by controlling upstream turbines improves power output and lowers operating costs. The optimal solution to improve LCOE is to achieve rated power without experiencing wear from operation, which is infeasible with the current O&M models. Because LCOE behaves like $1/x$ below rated power, any control action that reduces capacity factor leads to a sharp increase in LCOE. Since turbine power scales with U^3, operating costs would have to decrease faster than U^3 or else decline with increasing wind speed above rated power. Replacing the L_{10} or F_T O&M models with a descriptive function for each turbine type based on local maintenance records would enable new avenues for optimizing operating costs above rated power. Furthermore, the economic values used in this study are regional or national averages. Incorporating operator-specific CapEx and lifetime OpEx into the optimization would allow the optimizer to better tailor turbine operation to individual plants.

IV. CONCLUSIONS

EWLs were presented for neighboring plants within the AWAKEN project. Results were obtained from FLORIS simulations for each of the five plants in the study area. Simulations were performed based on measured atmospheric conditions using the GCH and TurbOPark wake models with turbine models created in WISDEM/WEIS. Multiplant wake interactions are shaped by plant power density, distance between neighboring plants, and regional atmospheric conditions. Because wind plants are designed around expected inflow conditions, wake losses are unevenly distributed among plants. Plants located along the most common wind direction experience a disproportionate amount of external wake losses.

Wake steering and axial induction were evaluated in FLORIS as control strategies for plant operators to mitigate external wake losses. Two optimization cost functions were considered, one based on EWL and the other on EWL-driven LCOE costs. LCOE optimizations also included two models for turbine O&M costs. Neither strategy was able to reduce EWL or improve LCOE when balancing the losses between upstream plants with the benefits of their downstream neighbors. Neglecting the losses from upstream plants revealed wake steering and axial induction can reduce plant wakes, although these strategies were ill-suited for improving regional performance. Improving bearing lifetime and reducing turbine loads are viable avenues for improving LCOE, although the precise benefit for a given plant depends on detailed economic information which is not readily accessible.

As implemented in contemporary engineering wake models, control strategies are limited to scenarios where individual turbine wakes are the dominant flow feature. Yaw-based wake steering is feasible when plant spacing is sufficiently dense to where all wakes may be treated as internal wake or when atmospheric conditions allow single wakes to persist far downstream. However, wake steering is limited by plant geometry since plant wakes can span several kilometers, while

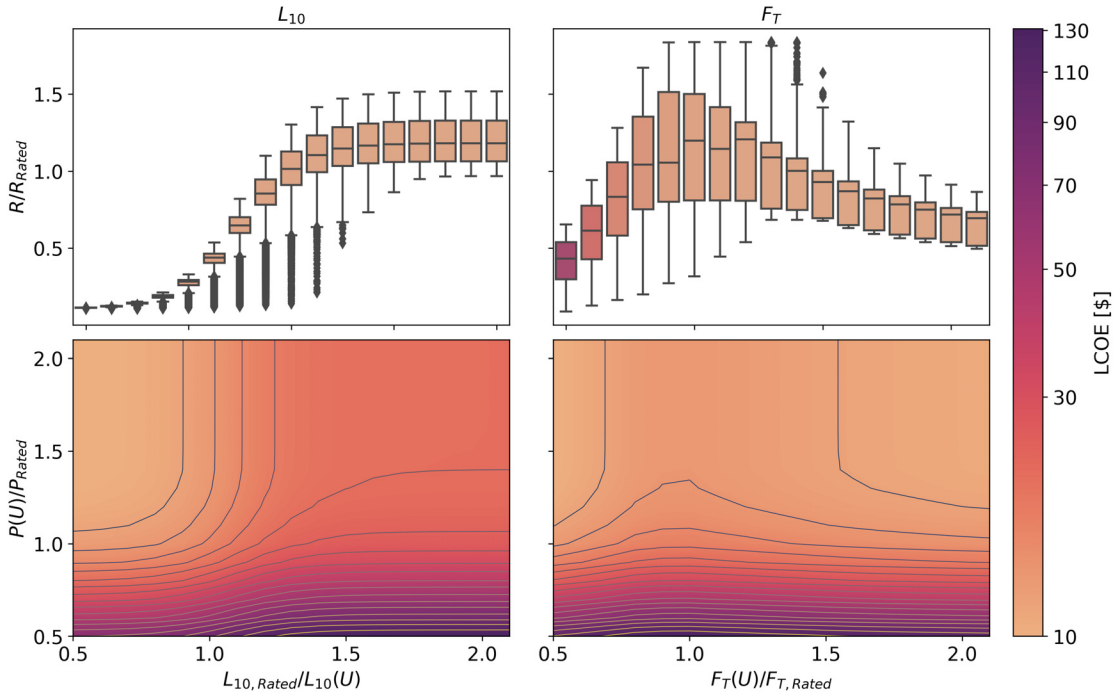

FIG. 8. Normalized L_{10} (top left) and F_T (top right) with corresponding LCOE optimization surfaces (bottom) for all baseline FLORIS simulations. R/R_{Rated} denotes bearing lifetime or rotor-averaged thrust force relative to the average value at rated velocity. Contour spacing indicates the rate of change in LCOE relative to rated operation as a function of power and O&M costs.

typical wake displacement from yaw is on the order of rotor diameter. Axial induction control is a poor candidate for mitigating plant wake losses as it requires curtailing an unreasonable portion of upstream plants. High-fidelity simulations that include plant-scale flow features and SCADA from operating wind plants are needed to confirm if the findings reported here are a consequence of controls implementation in current engineering wake models or the control strategies themselves.

Nonetheless, addressing losses from neighboring plants is likely to become a significant driver of plant design and operating strategy as installed wind plant density increases. New approaches are needed to consider plant interactions at the regional scale that balance physical fidelity with computational feasibility. The development of plant-level engineering wake models that include relevant physics, such as blockage, local speedup, aggregate wake merging, and plant boundary layer formation, may allow future efforts to identify opportunities to optimize plant performance. We anticipate the ideas and approach developed here will help direct future efforts to focus on improving the relationship between turbine operation and costs; modeling aggregate wind plant wakes; and designing optimal wind plants.

ACKNOWLEDGMENTS

This work was authored in part by the National Renewable Energy Laboratory, operated by Alliance for Sustainable Energy, LLC, for the U.S. Department of Energy (DOE) under Contract No. DE-AC36-08GO28308. Funding provided by the Department of Energy Office of Energy Efficiency and Renewable Energy Wind Energy Technologies Office. The views expressed in the article do not necessarily represent the views of the DOE or the U.S. Government. The U.S. Government retains and the publisher, by accepting the article for publication, acknowledges that the U.S. Government retains a nonexclusive, paid-up, irrevocable, worldwide license to publish or reproduce the published form of this work, or allow others to do so, for U.S. Government purposes.

A portion of this research was performed using computational resources sponsored by the Department of Energy's Office of Energy Efficiency and Renewable Energy and located at the National Renewable Energy Laboratory.

AUTHOR DECLARATIONS

Conflict of Interest

The authors have no conflicts to disclose.

Author Contributions

Ryan Scott: Conceptualization (equal); Formal analysis (equal); Methodology (equal); Software (equal); Visualization (equal); Writing – original draft (lead). **Nicholas Hamilton:** Conceptualization (equal); Methodology (equal); Project administration (equal); Resources (equal); Supervision (equal); Writing – review & editing (equal). **Raúl Bayoán Cal:** Conceptualization (equal); Methodology (equal); Project administration (equal); Supervision (equal); Writing – review &

editing (equal). **Patrick Moriarty:** Funding acquisition (lead); Project administration (equal); Resources (equal); Supervision (equal); Writing – review & editing (equal).

DATA AVAILABILITY

The data that support the findings of this study are available from the corresponding author upon reasonable request.

REFERENCES

[1]IEA, *World Energy Outlook 2022* (IEA, 2022).
[2]R. Wiser, M. Bolinger, B. Hoen, D. Millstein, J. Rand, G. Barbose, N. Darghouth, W. Gorman, S. Jeong, and B. Paulos, *Land-Based Wind Market Report: 2022 Edition* (Lawrence Berkeley National Lab., Berkeley, CA, 2022).
[3]J. K. Lundquist, K. K. DuVivier, D. Kaffine, and J. M. Tomaszewski, "Costs and consequences of wind turbine wake effects arising from uncoordinated wind energy development," Nat. Energy **4**, 26–34 (2019).
[4]B. Cañadillas, R. Foreman, V. Barth, S. Siedersleben, A. Lampert, A. Platis, B. Djath, J. Schulz-Stellenfleth, J. Bange, S. Emeis *et al.*, "Offshore wind farm wake recovery: Airborne measurements and its representation in engineering models," Wind Energy **23**, 1249–1265 (2020).
[5]J. Schneemann, A. Rott, M. Dörenkämper, G. Steinfeld, and M. Kühn, "Cluster wakes impact on a far-distant offshore wind farm's power," Wind Energy Sci. **5**, 29–49 (2020).
[6]N. G. Nygaard and S. D. Hansen, "Wake effects between two neighbouring wind farms," J. Phys.: Conf. Ser. **753**, 032020 (2016).
[7]N. G. Nygaard, S. T. Steen, L. Poulsen, and J. G. Pedersen, "Modelling cluster wakes and wind farm blockage," J. Phys.: Conf. Ser. **1618**, 062072 (2020).
[8]F. Porté-Agel, M. Bastankhah, and S. Shamsoddin, "Wind-turbine and wind-farm flows: A review," Boundary-Layer Meteorol. **174**, 1–59 (2020).
[9]A. Stieren and R. J. Stevens, "Impact of wind farm wakes on flow structures in and around downstream wind farms," Flow **2**, E21 (2022).
[10]B. Foloppe, L. Dewitte, and W. Munters, "Exploring cooperation between wind farms: A wake steering optimization study of the Belgian offshore wind farm cluster," J. Phys.: Conf. Ser. **2505**, 012055 (2023).
[11]R. J. Foreman, B. Cañadillas, and N. Robinson, "The atmospheric stability dependence of far wakes on the power output of downstream wind farms," Energies **17**, 488 (2024).
[12]M. Kelly, G. Larsen, N. K. Dimitrov, and A. Natarajan, "Probabilistic meteorological characterization for turbine loads," J. Phys.: Conf. Ser. **524**, 012076 (2014).
[13]N. Dimitrov, A. Natarajan, and J. Mann, "Effects of normal and extreme turbulence spectral parameters on wind turbine loads," Renewable Energy **101**, 1180–1193 (2017).
[14]A. M. M. Ismaiel and S. Yosida, "Study of turbulence intensity effect on the fatigue lifetime of wind turbines," Evergreen: Jt. J. Novel Carbon Resour. Sci. Green Asia Strategy **5**, 25–32 (2018).
[15]C. E. Clark, G. Barter, K. Shaler, and B. DuPont, "Reliability-based layout optimization in offshore wind energy systems," Wind Energy **25**, 125–148 (2022).
[16]A. Natarajan, "Damage equivalent load synthesis and stochastic extrapolation for fatigue life validation," Wind Energy Sci. **7**, 1171–1181 (2022).
[17]A. P. Stanley, J. King, C. Bay, and A. Ning, "A model to calculate fatigue damage caused by partial waking during wind farm optimization," Wind Energy Sci. **7**, 433–454 (2022).
[18]R. Scott, B. Viggiano, T. Dib, N. Ali, M. Hölling, J. Peinke, and R. B. Cal, "Wind turbine partial wake merging description and quantification," Wind Energy **23**, 1610–1618 (2020).
[19]P. McKay, R. Carriveau, and D. S.-K. Ting, "Wake impacts on downstream wind turbine performance and yaw alignment," Wind Energy **16**, 221–234 (2013).
[20]F. Campagnolo, V. Petrović, J. Schreiber, E. M. Nanos, A. Croce, and C. L. Bottasso, "Wind tunnel testing of a closed-loop wake deflection controller for wind farm power maximization," J. Phys.: Conf. Ser. **753**, 032006 (2016).
[21]M. Bastankhah and F. Porté-Agel, "Wind farm power optimization via yaw angle control: A wind tunnel study," J. Renewable Sustainable Energy **11**, 023301 (2019).
[22]E. Simley, P. Fleming, N. Girard, L. Alloin, E. Godefroy, and T. Duc, "Results from a wake-steering experiment at a commercial wind plant: Investigating the wind speed dependence of wake-steering performance," Wind Energy Sci. **6**, 1427–1453 (2021).
[23]M. Debnath, A. K. Scholbrock, D. Zalkind, P. Moriarty, E. Simley, N. Hamilton, C. Ivanov, R. S. Arthur, R. Barthelmie, N. Bodini *et al.*, "Design of the American wake experiment (AWAKEN) field campaign," J. Phys.: Conf. Ser. **2265**, 022058 (2022).
[24]J. Meyers, C. Bottasso, K. Dykes, P. Fleming, P. Gebraad, G. Giebel, T. Göçmen, and J.-W. van Wingerden, "Wind farm flow control: Prospects and challenges," Wind Energy Sci. Discuss. **7**, 2271–2306 (2022).
[25]E. Simley, D. Millstein, S. Jeong, and P. Fleming, "The value of wake steering wind farm control in US energy markets," Wind Energy Sci. Discuss. **9**, 219–234 (2024).
[26]W. Munters and J. Meyers, "Towards practical dynamic induction control of wind farms: Analysis of optimally controlled wind-farm boundary layers and sinusoidal induction control of first-row turbines," Wind Energy Sci. **3**, 409–425 (2018).
[27]J. A. Frederik, B. M. Doekemeijer, S. P. Mulders, and J.-W. van Wingerden, "The helix approach: Using dynamic individual pitch control to enhance wake mixing in wind farms," Wind Energy **23**, 1739–1751 (2020).
[28]E. Bossanyi, G. C. Larsen, and M. M. Pedersen, "Full-scale validation of optimal axial induction control of a row of turbines at Lillgrund wind farm," J. Phys.: Conf. Ser. **2505**, 012042 (2023).
[29]D. van der Hoek, B. V. d Abbeele, C. S. Ferreira, and J.-W. van Wingerden, "Maximizing wind farm power output with the helix approach—Experimental validation and wake analysis using tomographic PIV," arXiv:2306.12849 (2023).
[30]T. Stehly and P. Duffy, "2020 cost of wind energy review," Report No. NREL/TP-5000-81209 [National Renewable Energy Lab. (NREL), Golden, CO, 2021].
[31]N. Hamilton, C. J. Bay, P. Fleming, J. King, and L. A. Martínez-Tossas, "Comparison of modular analytical wake models to the Lillgrund wind plant," J. Renewable Sustainable Energy **12**, 053311 (2020).
[32]E. Branlard, E. Quon, A. R. M. Forsting, J. King, and P. Moriarty, "Wind farm blockage effects: Comparison of different engineering models," J. Phys.: Conf. Ser. **1618**, 062036 (2020).
[33]NREL, *Floris. Version 3.1* (NREL, 2022).
[34]P. Moriarty, N. Hamilton, M. Debnath, T. Herges, B. Isom, J. K. Lundquist, D. Maniaci, B. Naughton, R. Pauly *et al.*, "American wake experiment (AWAKEN)," Report No. LLNL-TR-806278; NREL/TP-5000-75789; SAND-2020-4296 (Lawrence Livermore National Lab., Livermore, CA, 2020).
[35]B. Hoen, J. Diffendorfer, J. Rand, L. Kramer, C. Garrity, and H. Hunt, "United States wind turbine database (v7.0)," U.S. Geological Survey, American Clean Power Association, and Lawrence Berkeley National Laboratory data release (2024).
[36]NREL, "OpenFAST turbine models," GitHub (2022), https://github.com/NREL/openfast-turbine-models.
[37]NREL, "WISDEM/WEIS," v1.0, GitHub (2022), https://github.com/WISDEM/WEIS.
[38]K. Gaustad and S. Xie, "Best-estimate fluxes from EBBR measurements and bulk aerodynamics calculations (30BAEBBR)," Atmospheric Radiation Measurement (ARM) user facility (2022).
[39]A. Koontz, S. Biraud, and S. Chan, "Carbon dioxide flux measurement systems (CO2FLX25M)," Atmospheric Radiation Measurement (ARM) user facility (2022).
[40]A. Koontz, S. Biraud, S. Biraud, and S. Chan, "Carbon dioxide flux measurement systems (CO2FLX60M)," Atmospheric Radiation Measurement (ARM) user facility (2022).
[41]T. Shippert, R. Newsom, L. Riihimaki, and D. Zhang, "Doppler LIDAR horizontal wind profiles (DLPROFWIND4NEWS)," Atmospheric Radiation Measurement (ARM) user facility (2022).
[42]M. Jensen, S. Giangrande, T. Fairless, and A. Zhou, "Interpolated sonde (interpolated sonde)," Atmospheric Radiation Measurement (ARM) user facility (2022).
[43]E. Keeler, J. Kyrouac, and B. Ermold, "Automatic weather station (MAWS)," Atmospheric Radiation Measurement (ARM) user facility (2022).

[44]J. Kyrouac, Y. Shi, and M. Tuftedal, "Surface meteorological instrumentation (MET)," Atmospheric Radiation Measurement (ARM) user facility (2022).
[45]R. Krishnamurthy, R. K. Newsom, D. Chand, and W. J. Shaw, "Boundary layer climatology at arm southern great plains," Report No. PNNL-30832 (Pacific Northwest National Lab., 2021).
[46]International Organization for Standardization, *Rolling Bearings: Dynamic Load Ratings and Rating Life* (International Organization for Standardization, 1990).
[47]International Organization for Standardization, *Rolling Bearings: Dynamic Load Ratings and Rating Life* (International Organization for Standardization, 2007).
[48]E. V. Zaretsky, "Rolling bearing life prediction, theory, and application," Report No. NASA/TP-2013-215305 (NASA, 2013).
[49]N. Nygaard, L. Poulsen, E. Svensson, and J. Pedersen, "Large-scale benchmarking of wake models for offshore wind farms," J. Phys.: Conf. Ser. **2265**, 022008 (2022).
[50]J. King, P. Fleming, R. King, L. A. Martínez-Tossas, C. J. Bay, R. Mudafort, and E. Simley, "Control-oriented model for secondary effects of wake steering," Wind Energy Sci. **6**, 701–714 (2021).
[51]M. Bastankhah and F. Porté-Agel, "A new analytical model for wind-turbine wakes," Renewable Energy **70**, 116–123 (2014).
[52]M. Bastankhah and F. Porté-Agel, "Experimental and theoretical study of wind turbine wakes in yawed conditions," J. Fluid Mech. **806**, 506–541 (2016).
[53]L. A. Martínez-Tossas, J. Annoni, P. A. Fleming, and M. J. Churchfield, "The aerodynamics of the curled wake: A simplified model in view of flow control," Wind Energy Sci. **4**, 127–138 (2019).
[54]L. A. Martínez-Tossas, J. King, E. Quon, C. J. Bay, R. Mudafort, N. Hamilton, M. F. Howland, and P. A. Fleming, "The curled wake model: A three-dimensional and extremely fast steady-state wake solver for wind plant flows," Wind Energy Sci. **6**, 555–570 (2021).
[55]N. O. Jensen, *A Note on Wind Generator Interaction* (Risø National Laboratory, 1983).
[56]R. H. Byrd, P. Lu, J. Nocedal, and C. Zhu, "A limited memory algorithm for bound constrained optimization," SIAM J. Sci. Comput. **16**, 1190–1208 (1995).
[57]C. Zhu, R. H. Byrd, P. Lu, and J. Nocedal, "Algorithm 778: L-BFGS-B: Fortran subroutines for large-scale bound-constrained optimization," ACM Trans. Math. Software **23**, 550–560 (1997).
[58]P. Virtanen, R. Gommers, T. E. Oliphant, M. Haberland, T. Reddy, D. Cournapeau, E. Burovski, P. Peterson, W. Weckesser, J. Bright, S. J. van der Walt, M. Brett, J. Wilson, K. J. Millman, N. Mayorov, A. R. J. Nelson, E. Jones, R. Kern, E. Larson, C. J. Carey, İ. Polat, Y. Feng, E. W. Moore, J. VanderPlas, D. Laxalde, J. Perktold, R. Cimrman, I. Henriksen, E. A. Quintero, C. R. Harris, A. M. Archibald, A. H. Ribeiro, F. Pedregosa, P. van Mulbregt, and SciPy 1.0 Contributors, "SciPy 1.0: Fundamental algorithms for scientific computing in Python," Nat. Methods **17**, 261–272 (2020).
[59]NREL and G. Starke, "Floris. Version 3.1 variable CT feature," v3.1, GitHub (2022), https://github.com/genevievestarke/floris/tree/feature/variable_ct.